Optics Letters

Self-pulsations in a microcavity Brillouin laser

Yingchun Qin,[1,†] Shulin Ding,[1,6,†] Shujian Lei,[1] Jie Liu,[1] Yan Bai,[1] Menghua Zhang,[1] Yuhang Li,[2,3] Jianming Wen,[4] Xiaoshun Jiang,[1,*] and Min Xiao[1,5]

[1]National Laboratory of Solid State Microstructures, College of Engineering and Applied Sciences and School of Physics, Nanjing University, Nanjing 210093, China
[2]Key Laboratory of Photonic Control Technology (Tsinghua University), Ministry of Education, Beijing 100084, China
[3]State Key Laboratory of Precision Measurement Technology and Instruments, Tsinghua University, Beijing 100084, China
[4]Department of Physics, Kennesaw State University, Marietta, Georgia 30060, USA
[5]Department of Physics, University of Arkansas, Fayetteville, Arkansas 72701, USA
[6]e-mail: dingsl@nju.edu.cn
*Corresponding author: jxs@nju.edu.cn
†These authors contributed equally to this Letter.

Received 16 August 2021; revised 5 November 2021; accepted 15 November 2021; posted 18 November 2021; published 13 January 2022

We demonstrate a new, to the best of our knowledge, kind of self-pulsation in a microcavity Brillouin laser. This specific self-pulsation is generated by the interplay between the Brillouin lasing and the thermo-optic effect in an optical microcavity. Intriguingly, the self-pulsation behaviors are simultaneously present in both forward input pump and backward Brillouin lasing emission. By developing a coupled-mode theory, our numerical simulations display an excellent agreement with the experimental results.

https://doi.org/10.1364/OL.440677

Whispering gallery mode (WGM) microresonators with high quality-factor (Q-factor) have propelled tremendous progress across cavity optomechanics [1], non-Hermitian photonics [2–4], Kerr microcombs [5,6], narrow-linewidth lasers [7–10], and sensors [11]. Among them, optical-microcavity-based Brillouin lasers have emerged as a remarkable candidate for integrated ultranarrow linewidth lasers [7–9], thereby advancing many applications such as microwave photonics [12], integrated microgyroscopes [13,14], and the generation of high-performance optical frequency combs [15].

It is known that during microcavity Brillouin lasing, the thermo-optic effect [16,17] is often used to stabilize the pump frequency detuning [18]. This thermo-optic effect has also been used for designing Raman microlasers [19], rare-earth-doped microlasers [20–22], optical harmonics [23,24], and Kerr microcombs [25]. If at the same time there exist other nonlinear effects, like optical Kerr nonlinearity [26–28], photorefractive effect [29], free-carrier-induced nonlinearity [30,31], or additional thermo-optic nonlinearity in a coated layer [32,33], peculiar self-pulsations may be induced amongst the output signals [34].

Here, we report the observation of self-pulsations in a Brillouin lasing process induced by the interaction between the Brillouin lasing and the thermo-optic nonlinearity in a high-Q silica optical microresonator. Unlike previously reported results in an optical microcavity [27,28,33], the newly observed self-pulsations stem from the interplay between the lasing process and the thermo-optic effect. We note that in previous work, such an interplay has been used in a fiber Brillouin laser system to stabilize the laser frequency [35].

Figure 1(a) is the schematic diagram of our experimental set-up. A tunable external-cavity diode laser at 1550 nm is used to excite a chip-based silica microtoroid resonator [36]. Then, a silica fiber taper is used to couple the light into and out of the microresonator. The transmitted pump light and back-propagating Brillouin signals are fed to two separate photodetectors via an optical circulator. Figure 1(b) shows the optical image of the fabricated microtoroid resonator with a major diameter of 3.35 mm and a minor diameter of approximately 45.5 μm. Because the free spectral range (FSR) of the cavity at ~1550 nm is approximately 18 GHz (much larger than the Brillouin acoustic frequency), the demanded phase-matching condition is realized by making use of two optical modes from different transverse mode families. The employed pump and Brillouin modes have intrinsic Q-factors of 1.60×10^8 and 3.52×10^8, and loaded Q-factors of about 6.94×10^7 and 1.42×10^8, respectively. Figure 1(c) illustrates the measured optical spectrum of the Brillouin laser with a frequency shift of approximately 11.3 GHz. Experimentally, when the pump light is set above a certain power, striking self-pulsations take place in both the transmitted pump beam and generated Brillouin laser waves.

These self-pulsations can be intuitively understood with the four basic processes depicted in Fig. 2. Because the response time of the stimulated Brillouin scattering (SBS) is much shorter than that of the thermo-optic effect, the Brillouin lasing process is first initiated; meanwhile, the generated Stokes field starts to grow especially when the system is lifted above the threshold of the Brillouin lasing (see Process I). Then, owing to the intracavity energy spectra of both the pump and Brillouin modes that are altered during the Brillouin lasing [37], the total intracavity optical energy will become increased for a frequency detuned pump. As a result, the microcavity is getting heated because of optical absorption during the generation of the Brillouin laser. Accordingly, the cavity resonances are steadily redshifted and result in an increase of the effective pump frequency detuning

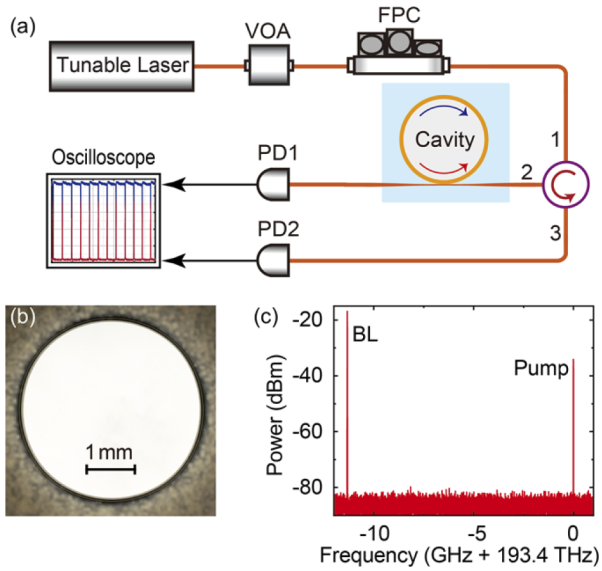

Fig. 1. (a) Schematic illustration of the experimental set-up. VOA, variable optical attenuator; FPC, fiber polarization controller; PD, photodetector. The circle labeled with 3 ports is an optical circulator. (b) Photograph of the silica microtoroid used in the experiment. (c) Optical spectrum of the Brillouin laser (BL) and scattered pump laser in the backward direction.

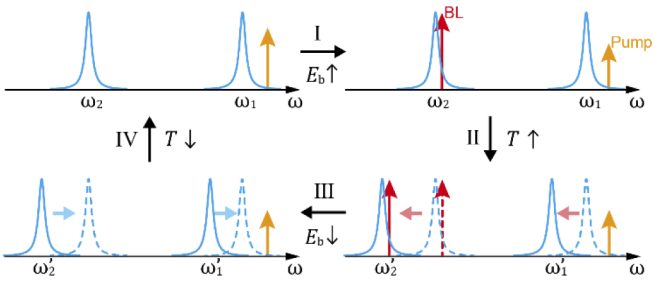

Fig. 2. Schematic diagram of self-pulsations in a microcavity Brillouin laser system. The vertical arrows stand for pump (or Brillouin, BL) laser in frequency domain. Here, ω_1 (ω_1') and ω_2 (ω_2') stand for the resonant frequencies of the pump mode and the resonant frequency of Brillouin modes before (after) the cavity heated by the Brillouin laser, respectively, and T and E_b represent the cavity temperature and the intracavity optical energy of the Brillouin wave. See the main text for details.

(see Process II). Subsequently, the Stokes field is slowly varied along with the change of the pump frequency detuning. However, owing to the limited range of the effective pump detuning with the existence of the Brillouin laser, the Brillouin lasing can be extinguished (see Process III) when the pump laser is far detuned from the resonance. The disappearance of the Brillouin lasing eventually leads to the cavity cooling down (see Process IV) and then resets the cavity resonance back to the initial value, whereby it is ready for the next cycle of the self-pulsation.

To theoretically understand the mechanism of the observed self-pulsations in the microcavity-based Brillouin laser, we begin with the modelling of the thermo-optic effect [17]. As known, when the cavity is excited with a certain power, the cavity mode will become heated. The heat will diffuse to the bulk and surroundings of the cavity. Subsequently, the temperature growth will shift the resonant frequencies of the cavity modes by thermally changing the refraction indices of the material. Considering this effect, we can express the overall frequency shifts, induced by the thermo-optic effect, of both the pump and Brillouin modes as

$$\Delta\omega_j = \beta_j \Delta T, \tag{1}$$

where $j = 1, 2$ are referred to the pump and Brillouin modes, respectively. In Eq. (1), β_j are the coefficients of thermally induced frequency drifts of the cavity modes and ΔT stands for the temperature variation.

Next, we consider the Brillouin lasing process [38] associated with the thermo-optic effect. Because the generation of the Brillouin laser can be strongly affected by the Kerr nonlinear effect, this prompts us to further analyze the Kerr self-phase modulations of both pump and Brillouin modes [15]. As such, we develop a set of coupled-mode equations to describe the dynamics of the three modes (two optical and one acoustic),

$$\frac{da_1}{dt} = \left(-i\Delta\omega_p + i\beta_1\Delta T - ig_{k,1}|a_1|^2 - \frac{\gamma_1}{2}\right)a_1 - ig_b a_2 b + \sqrt{\kappa_1}s_{in}, \tag{2}$$

$$\frac{da_2}{dt} = \left(-i\Delta\omega_b + i\beta_2\Delta T - ig_{k,2}|a_2|^2 - \frac{\gamma_2}{2}\right)a_2 - ig_b a_1 b^*, \tag{3}$$

$$\frac{db}{dt} = \left(-i\Delta\Omega_m - \frac{\gamma_m}{2}\right)b - ig_b a_1 a_2^*. \tag{4}$$

Here, a_j (b) denotes the amplitudes of the optical (acoustic) waves, s_{in} is the input pump field; $\Delta\omega_p = \omega_p - \omega_{0,1}$ represents the pump frequency detuning relative to the pump mode of cold cavity with ω_p and $\omega_{0,1}$, respectively, being the pump frequency and resonant frequency of cold pump mode; $\Delta\omega_b = \omega_b - \omega_{0,2}$ ($\Delta\Omega_m = \Omega_m - \Omega_0$) represents the frequency shift of the Brillouin optical (acoustic) waves with ω_b, (Ω_m) and $\omega_{0,2}(\Omega_0)$, respectively, being the frequency of the Stokes (acoustic) wave and the frequency of the cold Brillouin (acoustic) mode; $\gamma_j = \gamma_{0,j} + \kappa_j$ refers to the total decay rates of the optical mode in terms of the intrinsic decay rate $\gamma_{0,j}$ and the external coupling rates to the waveguide κ_j; $g_{k,j}$ is the self-phase modulation coefficient; and g_b stands for the coupling coefficient between the optical and acoustic modes in the Brillouin lasing process.

To characterize the thermal evolution of the system, we introduce the following dynamical equation of ΔT [17]:

$$\frac{d\Delta T}{dt} = -\frac{1}{\tau_T}\Delta T + c_{T,1}|a_1|^2 + c_{T,2}|a_2|^2, \tag{5}$$

where τ_T is the overall thermal relaxation rate to the ambient temperature, and $c_{T,j} = \gamma_{abs,j}/t_r$ with $\gamma_{abs,j}$ standing for the coefficient of thermal absorption and $t_r = n_0 L_{eff}/c$ is the cavity round-trip time.

With these, we further use the following relations to calculate the forward and backward output fields:

$$s_{out,f} = s_{in} - \sqrt{\kappa_1}a_1, \tag{6}$$

$$s_{out,b} = \sqrt{\kappa_2}a_2, \tag{7}$$

with $s_{out,f}$ and $s_{out,b}$ being the amplitudes of the forward and backward optical fields, respectively.

Figure 3(a) illustrates typical temporal traces measured for the transmitted pump and generated Brillouin laser signals at fixed pump frequency and the input power of ~40 mW. From these time traces, one can see that both the transmitted forward pump and the generated backward Brillouin laser exhibit oscillatory

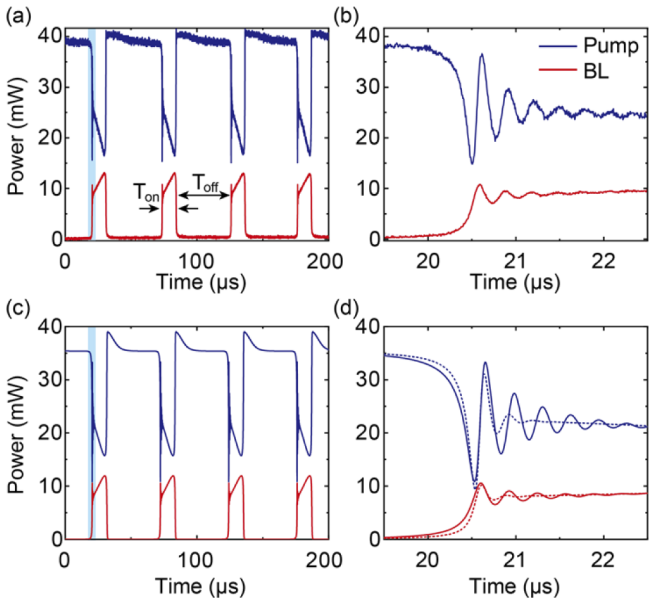

Fig. 3. (a), (b) Typically observed time traces of self-pulsations observed in experiments. (c), (d) Numerically simulated self-pulsations corresponding to (a) and (b). Upper lines, transmitted pump laser signals; lower lines, backward Brillouin laser signals. Parts (b) and (d) are enlarged views of the shaded areas in (a) and (c). Here, T_{on} and T_{off} in (a) mark the temporal lengths with and without Brillouin lasing in one cycle of the self-pulsation. In (d), dashed lines are the numerically simulated self-pulsation without the Kerr effect.

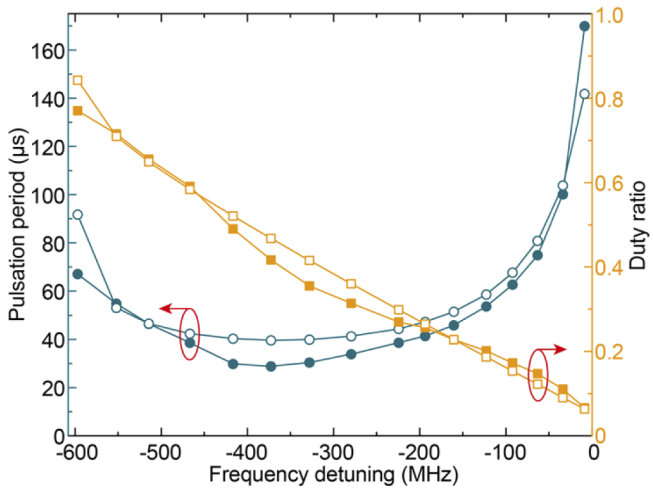

Fig. 4. Pulsation periods (circles) and duty ratios (squares) of the generated self-pulsing Brillouin laser as a function of the pump detuning (corresponding to the cold cavity). Solid marks are measured experimental results, whereas hollow marks are numerical simulations.

patterns with the time period of 52 μs. Our results show that this oscillatory behavior of the transmitted pump laser originates from the periodical thermal motion of the pump mode, which is induced by the self-pulsations of the Brillouin laser.

To confirm the experimental results, we numerically solve Eqs. (1)–(7) with the following physical parameters: $\gamma_{0,1} = 2\pi \times 1.21$ MHz, $\gamma_{0,2} = 2\pi \times 0.55$ MHz, $\kappa_1 = 2\pi \times 1.58$ MHz, $\kappa_2 = 2\pi \times 0.81$ MHz, $\gamma_m = 2\pi \times 40$ MHz, and the input pump power P = 40 mW. We further set the resonant frequency mismatch among three modes to be $\Delta\omega_0 = \omega_1 - \omega_2 - \Omega_0 = 2\pi \times 70$ MHz. Additionally, we adopt the following formulas [5,39] to evaluate the nonlinear coupling coefficients for the stimulated Brillouin process as well as the Kerr nonlinear effect:

$$g_b^2 = \frac{G_b c^2 \gamma_m \Lambda}{2 n_0^2 V_{eff,1}}, \tag{8}$$

$$g_{k,j} = \frac{n_2 c \omega_j}{n_0^2 V_{eff,j}}. \tag{9}$$

Here, G_b is the bulky Brillouin centerline gain coefficient, $n_0 = 1.45$ and $n_2 = 2.6 \times 10^{-20}$ m^2/W are respectively the linear and nonlinear refractive indices of silica, $V_{eff,j} = A_{eff,j} L_{eff}$ is the effective mode volume with L_{eff} and $A_{eff,j}$ being the effective mode length and area, Λ is the spatial overlap between the optical modes and acoustic mode, and c is the light speed in vacuum. In this work, we find $V_{eff,1} \approx 1.7 \times 10^{-13}$ m^3 and $V_{eff,2} \approx 8.4 \times 10^{-13}$ m^3 with $A_{eff,1} = 16$ μm^2, $A_{eff,2} = 80$ μm^2, and $L_{eff} = \pi \times 3.35$ mm, which are close to the simulated results based on the finite element method. In the numerical simulation, we further choose $G_b = 4.32 \times 10^{-12}$ m/W [39], $\Lambda = 0.2$, $\gamma_{abs,1} = 93.1$ K/J (which is reasonable according to Ref. [26]), $\gamma_{abs,2} = 15.0$ K/J, and $\tau_T = 1.2$ ms to fit the experimental data. Here, $\beta_1 = \beta_2 = -2\pi \times 1.37$ GHz/K are experimentally extracted by measuring the resonance frequency shift with different temperatures of the sample [10]. The numerical simulations in Figs. 3(c) and 3(d) are obtained by adopting the fourth-order Runge–Kutta algorithm to solve Eqs. (2)–(5), in addition to the output signals calculated by Eqs. (6) and (7). It is apparent that our simulations match with the experimental results in an excellent way. Note that Fig. 3(b) is the zoom-in view of shaded area in Fig. 3(a), which displays a ringing-like line shape. According to numerical simulations [see Fig. 3(d)], we attribute this phenomenon to the fast self-phase modulations of the cavity field caused by the Kerr nonlinearities and the fast phase shifts induced by SBS-induced index change during the process of Brillouin laser generation [37,40]. As a comparison, we also perform simulations without the Kerr effect [dashed lines in Fig. 3(d)]. Interestingly, the ringing-like features simply induced by the SBS-induced index change are still observable but with slightly reduced amplitudes as well as reduced number of oscillation periods.

In the experiment, when fixing the input pump power and the loaded optical Q-factors, we find that the periods of the self-pulsations vary with the pump frequency. Alternatively, the repetition rate of the generated self-pulsing Brillouin laser is determined by the pump frequency detuning. As shown in Fig. 4, the measured oscillation periods first decrease from ~160 μs to ~30 μs and then gradually increase up to 100 μs when reducing the pump frequency. This trend is well explained by our numerical results. We attribute the decrease of the period to the fact that less time is needed to turn off the Brillouin lasing using the thermo-optic effect when the effective pump detuning is increased by increasing the pump frequency. In addition, the increase of the period comes from the smaller Brillouin gain as the effective pump detuning is too large. Consequently, more time is needed to excite the Brillouin laser after the Brillouin laser is turned off by the thermal-optic effect. During this process, we also notice that the duty ratios of the Brillouin laser pulses [$T_{on}/(T_{on} + T_{off})$, see Fig. 3(a)] decrease monotonically

from approximately 90% down to around 10% as the pump detuning becomes greater. Similarly, this is also because more time is needed to turn on the Brillouin laser in one cycle after it is turned off by the thermal-optic effect at the larger effective pump detuning. In the experiment, the measured self-pulsation threshold is approximately 2 mW for an optimized frequency detuning, which is smaller than the simulated results. This deviation may be attributed to the neglected difference of the thermally induced frequency drift between the pump and the Brillouin modes.

In conclusion, we have demonstrated a new kind of self-pulsation in an optical microcavity, which results from the competition between the Brillouin lasing process and the thermo-optic process. To confirm the experimental results, we have built a model to study this self-pulsation and achieved excellent agreement in between. The investigation on such self-pulsation is essential for constructing chip-based narrow-linewidth Brillouin lasers and Brillouin–Kerr soliton microcombs. In addition, the observed self-pulsation is expected to occur in other types of lasers, such as Raman or rare-earth-ion doped microlasers.

Funding. Guangdong Major Project of Basic and Applied Basic Research (2020B0301030009); National Natural Science Foundation of China (61922040); National Key Research and Development Program of China (2017YFA0303703); Fundamental Research Funds for the Central Universities (021314380189); National Science Foundation (1806519, EFMA-1741693); Kennesaw State University.

Disclosures. The authors declare no conflicts of interest.

Data availability. Data underlying the results presented in this paper are not publicly available at this time but may be obtained from the authors upon reasonable request.

REFERENCES

1. M. Aspelmeyer, T. J. Kippenberg, and F. Marquardt, Rev. Mod. Phys. **86**, 1391 (2014).
2. L. Chang, X. Jiang, S. Hua, C. Yang, J. Wen, L. Jiang, G. Li, G. Wang, and M. Xiao, Nat. Photonics **8**, 524 (2014).
3. B. Peng, S. K. Özdemir, F. Lei, F. Monifi, M. Gianfreda, G. L. Long, S. Fan, F. Nori, C. M. Bender, and L. Yang, Nat. Phys. **10**, 394 (2014).
4. J. Wen, X. Jiang, L. Jiang, and M. Xiao, J. Phys. B: At., Mol. Opt. Phys. **51**, 222001 (2018).
5. T. J. Kippenberg, A. L. Gaeta, M. Lipson, and M. L. Gorodetsky, Science **361**, eaan8083 (2018).
6. W. Wang, L. Wang, and W. Zhang, Adv. Photonics **2**, 1 (2020).
7. H. Lee, T. Chen, J. Li, K. Y. Yang, S. Jeon, O. Painter, and K. J. Vahala, Nat. Photonics **6**, 369 (2012).
8. W. Loh, A. A. S. Green, F. N. Baynes, D. C. Cole, F. J. Quinlan, H. Lee, K. J. Vahala, S. B. Papp, and S. A. Diddams, Optica **2**, 225 (2015).
9. S. Gundavarapu, G. M. Brodnik, M. Puckett, T. Huffman, D. Bose, R. Behunin, J. Wu, T. Qiu, C. Pinho, N. Chauhan, J. Nohava, P. T. Rakich, K. D. Nelson, M. Salit, and D. J. Blumenthal, Nat. Photonics **13**, 60 (2019).
10. W. Jin, Q.-F. Yang, L. Chang, B. Shen, H. Wang, M. A. Leal, L. Wu, M. Gao, A. Feshali, M. Paniccia, K. J. Vahala, and J. E. Bowers, Nat. Photonics **15**, 346 (2021).
11. X. Jiang, A. J. Qavi, S. H. Huang, and L. Yang, Matter **3**, 371 (2020).
12. B. J. Eggleton, C. G. Poulton, P. T. Rakich, M. J. Steel, and G. Bahl, Nat. Photonics **13**, 664 (2019).
13. J. Li, M.-G. Suh, and K. J. Vahala, Optica **4**, 346 (2017).
14. Y.-H. Lai, M.-G. Suh, Y.-K. Lu, B. Shen, Q.-F. Yang, H. Wang, J. Li, S. H. Lee, K. Y. Yang, and K. J. Vahala, Nat. Photonics **14**, 345 (2020).
15. Y. Bai, M. Zhang, Q. Shi, S. Ding, Y. Qin, Z. Xie, X. Jiang, and M. Xiao, Phys. Rev. Lett. **126**, 063901 (2021).
16. V. S. Ilchenko and M. L. Gorodetskii, Laser Phys. **2**, 1004 (1992).
17. T. Carmon, L. Yang, and K. J. Vahala, Opt. Express **12**, 4742 (2004).
18. M. Tomes and T. Carmon, Phys. Rev. Lett. **102**, 113601 (2009).
19. T. Carmon, T. J. Kippenberg, L. Yang, H. Rokhsari, S. Spillane, and K. J. Vahala, Opt. Express **13**, 3558 (2005).
20. A. Polman, B. Min, J. Kalkman, T. J. Kippenberg, and K. J. Vahala, Appl. Phys. Lett. **84**, 1037 (2004).
21. H. Fan, S. Hua, X. Jiang, and M. Xiao, Laser Phys. Lett. **10**, 105809 (2013).
22. H. Fan, X. Jiang, Y. Ding, and M. Xiao, Sci. China: Phys., Mech. Astron. **58**, 114204 (2015).
23. D. Farnesi, A. Barucci, G. C. Righini, S. Berneschi, S. Soria, and G. Nunzi Conti, Phys. Rev. Lett. **112**, 093901 (2014).
24. X.-X. Hu, J.-Q. Wang, Y.-H. Yang, J. B. Surya, Y.-L. Zhang, X.-B. Xu, M. Li, C.-H. Dong, G.-C. Guo, H. X. Tang, and C.-L. Zou, Opt. Express **28**, 11144 (2020).
25. T. Herr, V. Brasch, J. D. Jost, C. Y. Wang, N. M. Kondratiev, M. L. Gorodetsky, and T. J. Kippenberg, Nat. Photonics **8**, 145 (2014).
26. A. E. Fomin, M. L. Gorodetsky, I. S. Grudinin, and V. S. Ilchenko, J. Opt. Soc. Am. B **22**, 459 (2005).
27. Y.-S. Park and H. Wang, Opt. Lett. **32**, 3104 (2007).
28. L. Di Lauro, J. Li, D. J. Moss, R. Morandotti, S. T. Chu, M. Peccianti, and A. Pasquazi, Opt. Lett. **42**, 3407 (2017).
29. X. Sun, H. Liang, R. Luo, W. C. Jiang, X.-C. Zhang, and Q. Lin, Opt. Express **25**, 13504 (2017).
30. T. J. Johnson, M. Borselli, and O. Painter, Opt. Express **14**, 817 (2006).
31. D. M. Abrams, A. Slawik, and K. Srinivasan, Phys. Rev. Lett. **112**, 123901 (2014).
32. L. He, Y.-F. Xiao, J. Zhu, S. K. Ozdemir, and L. Yang, Opt. Express **17**, 9571 (2009).
33. Z.-C. Luo, C.-Y. Ma, B.-B. Li, and Y.-F. Xiao, AIP Adv. **4**, 122902 (2014).
34. X. Jiang and L. Yang, Light: Sci. Appl. **9**, 24 (2020).
35. O. Kotlicki and J. Scheuer, Opt. Express **25**, 27321 (2017).
36. J. Ma, X. Jiang, and M. Xiao, Photonics Res. **5**, B54 (2017).
37. D. A. Korobko, I. O. Zolotovskii, V. V. Svetukhin, A. V. Zhukov, A. N. Fomin, C. V. Borisova, and A. A. Fotiadi, Opt. Express **28**, 4962 (2020).
38. W. Loh, S. B. Papp, and S. A. Diddams, Phys. Rev. A **91**, 053843 (2015).
39. I. S. Grudinin, A. B. Matsko, and L. Maleki, Phys. Rev. Lett. **102**, 043902 (2009).
40. G. P. Agrawal, *Nonlinear Fiber Optics*, 4th ed. (Elsevier, 2013).